

# Breast Cancer Detection Based on Incremental Biochemical and Physiological Properties of Breast Cancers: A Six-Year, Two-Site Study<sup>1</sup>

Britton Chance, PhD, DSc, Shoko Nioka, MD, PhD, Jun Zhang, MS, Emily F. Conant, MD, Emily Hwang, MS, Susanne Briest, MD, Susan G. Orel, MD, Mitchell D. Schnall, MD, PhD, Brian J. Czerniecki, MD, PhD

**Rationale and Objectives.** To demonstrate that near-infrared spectroscopy would achieve sufficient sensitivity and specificity in human breast cancer to reach ROC/AUC values in the 90s and yet to warn of the potential liabilities of introduction of a novel technology in this field.

**Materials and Methods.** 116 subjects from two nations (44 were cancer-verified by biopsy and histopathology) were reviewed. NIR spectroscopy of total hemoglobin and its relative oxygenation were monitored in breast cancers and compared to their contralateral breast in a 2D nomogram for diagnostic evaluation. A novel handheld NIR breast cancer detector pad with a 3-wavelength LED and 8 detectors with 4 cm separation between source and detectors was placed on the subject's breast. The method is convenient, rapid, and safe and has achieved high patient compliance with minimal patient apprehension of compression, confinement, or radioactivity.

**Results.** The absorbance increments of the cancerous region are referred to the mirror image location on the contralateral breast. The two metrics are increased hemoglobin concentration due to angiogenesis and decreased hemoglobin saturation due to hypermetabolism of the cancer. The 2D nomogram display of these two metrics shows Zone 1 contains verified cancers and Zone 2 contains noncancers. ROC evaluation of the nomogram gives 95% AUC for the two sites, Philadelphia and Leipzig.

**Conclusion.** A simple, economical breast cancer detector has achieved high patient compliance and a high ROC/AUC score for a population which involved a range of tumors down to and including those of 0.8–1 cm in diameter.

**Key Words.** ROC/AUC; angiogenesis; hypermetabolism; breast cancer.

© AUR, 2005

This article describes the results of incremental biochemical and physiological properties of breast cancers with a

multi-wavelength, multi-detector breast cancer device. Whereas conventional studies emphasize incremental structural features such as spiculation and lobulation for diagnostics, little attention has been paid to incremental biochemical properties except using <sup>18</sup>FDOG in PET, which follows Otto Warburg's hypothesis of the predominance of glycolysis in cancer (1,2). Here we follow a derivative of the Warburg hypothesis emphasized by ourselves (3), namely that cancer has a normal complement of citric acid cycle and mitochondrial oxidative phosphorylation capacity but insufficient oxygen is delivered to the cancer, rendering it relatively hypoxic in spite of vigorous angiogenesis (4). In order to explore this hypothesis, we have developed a series of multi-wavelength, multi-detec-

*Acad Radiol* 2005; 12:925–933

<sup>1</sup> From the University of Pennsylvania, Departments of Biochemistry and Biophysics, 250 Anatomy/Chemistry Building, Philadelphia, PA 19104-6059 (B.C., S.N., J.Z., E.H.); Hospital of the University of Pennsylvania, Department of Radiology, Philadelphia, PA 19104 (E.F.C., S.G.O., M.D.S.); University of Leipzig, Department of Gynecology and Obstetrics, Leipzig, Germany (S.B.); University of Pennsylvania, Department of Surgery, Philadelphia, PA (B.J.C.). Received February 11, 2005; revision received April 28, 2005; revision accepted April 29. Supported by National Institutes of Health, National Cancer Institute No. CA87137; Pennsylvania Department of Health. **Address correspondence to:** B.C. e-mail: chance@mail.med.upenn.edu

© AUR, 2005

doi:10.1016/j.acra.2005.04.016

tor NIR devices (5,6) and for the past 6 years have dedicated one particular version of this development to breast cancer detection.

The optical method was used as early as 1929 by M. Cutler (7,8) to make shadow images of the breast (diaphanography) assuming that the cancer had different optical properties from the normal tissue and that a "shadowgram" could be made. This was a sound theory, but the differences are so small that the method was discredited in clinical trials. However, the understanding of the dual wavelength method (9–12), the photon diffusion in tissue (13) and the availability of monochromatic laser diodes, LED's and sensitive silicon diode detectors for the near infrared (NIR) regions (680-900 nm) has made possible quantification of the specific absorption of oxygenated and deoxygenated hemoglobin and of the total amount of hemoglobin within the breast cancer by reflectance spectroscopy (5,14).

Developing novel methods of detecting early, small cancers is the goal of NIH's cancer program (15), and this goal requires not only methods of high sensitivity/specificity in order to minimize undesirable false signals but also to afford a convenient, rapid, safe method with high patient compliance and minimal patient apprehensions of compression, confinement, and radioactivity. The development of NIR spectroscopy and imaging has proceeded rapidly since our early efforts (16) in this and other laboratories (17) and its usefulness has been tested in studies of the breast (18), brain (19), and muscle (20). Brain and muscle studies permit activation protocols in which the baseline is a low activity state for brain and a resting state for muscle. Baseline problems are minimized and incremental values of functional activation are obtained, particularly in event-related protocols (20). In the case of human breast tissue, functional activation is not available and instead spatial differences must be employed. Localization and characterization of the incremental changes of optical properties with respect to position changes seem necessary. Thus, the problem is significant and absolute values of optical properties involve problems of the physiological and biochemical baselines for distinguishing pathologies. In order to ameliorate that problem, we began to gather breast cancer data as an incremental study referenced to the mirror image location on the contralateral cancer-free breast (21,22) or, if necessary, a breast model (23,24).

In this investigation we used an NIR method which is capable of rapidly acquiring data from the human breast with a handheld puck (taking advantage of opto-electron-

ics miniaturization and retaining high quality functionality such as in cell phone technology (25)) that measures relative increases of tumor hemoglobin concentration and relative hemoglobin desaturation, all data being taken on a relative basis using generally the mirror image site on the contralateral breast, substantially mitigating the multiple effects of variable demographic and structural features of the human breast by measuring relative hemoglobin concentration and oxygenation compared to a normal breast within subjects. In analyzing relative hemoglobin concentration against relative saturation, a nomogram display conveniently segregates verified cancers from cancer-free breasts over a wide range of tumor sizes and types. received operating characteristic/area under the ROC curve (ROC/AUC) curves, positive predictive value (PPV), negative predictive value (NPV) and other information are displayed.

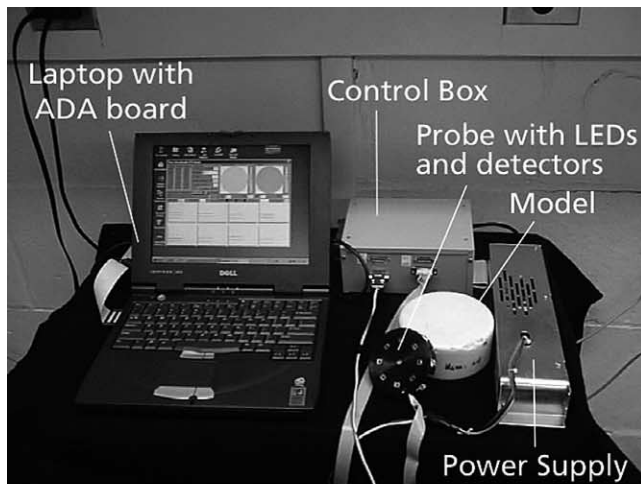
## MATERIALS AND METHODS

### Subjects

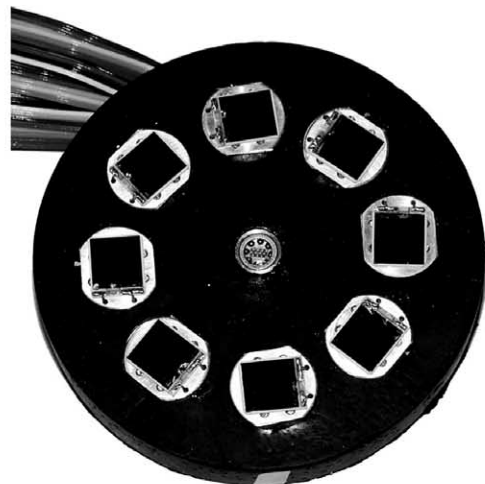
This study includes two clinical centers: the Abramson Family Cancer Research Institute/Department of Radiology of the Hospital of University of Pennsylvania (HUP), and the Department of Gynecology of Leipzig University. The population targeted at HUP is those who have come for possible biopsy and for radiology. The second group has come to the Breast Cancer Clinic at Leipzig. HUP and Leipzig provided 24 and 20 cancer patients, respectively, and 64 and 8 noncancer disease patients, respectively. Informed consent was obtained from all subjects participating in the study approved in the institutional review boards (IRB) of both the University of Pennsylvania and the University of Leipzig.

### Apparatus: NIR Spectrometer

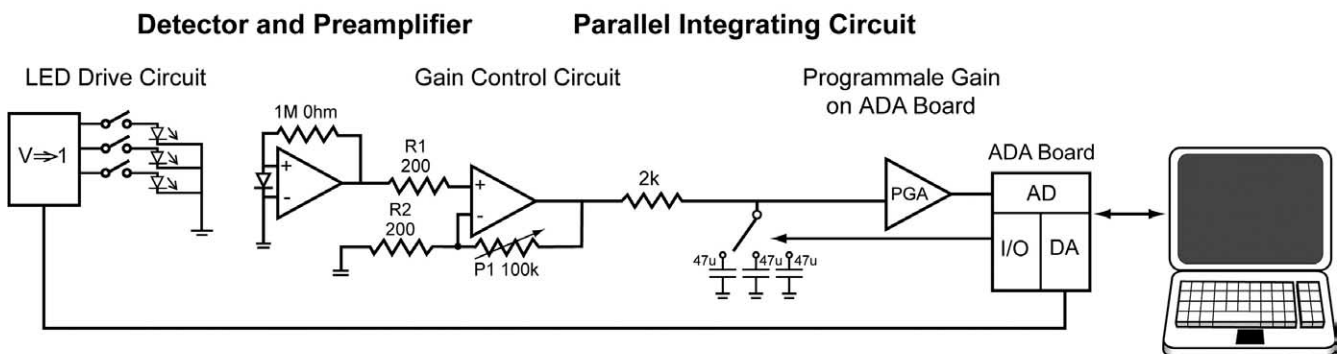
*Apparatus.*—We have used a continuous wave (CW) near-infrared spectrometer (NIRS) (Fig. 1A, B). In the center of the probe (Fig. 1B) is a 3-wavelength light-emitting diode (LED). The LED intensity is low, 10–15 mA. LEDs are not regulated by the FDA. This apparatus was used with a manual gain control for the first three years of the study and a digital gain control thereafter, but the device is considered to be substantially equivalent over the 6 years of study (27–29). The probe consisted of one multi-wavelength LED as a light source and 8 silicon diodes as detectors (Fig. 1). These 8 detectors surround



a.



b.



c.

**Figure 1.** A photograph of the whole apparatus (a) illustrates the handheld puck or probe, the coupling to the circuit box which contains the drivers for the LED, the amplifiers for the OPTI-101s, the digitally controlled gain adjustment amplifier, the electronic switch which decodes the light pulses and stores the information in a memory capacitor, the second set of switches which sample the memory capacitor at a rate compatible with the computer ADC, the software for computing blood concentration and blood saturation and the display on the computer which serves to normalize the signals through the digitally controlled amplifier (b). Handheld puck (c), which has 3 elements in series, gives a considerably narrow band wavelength at the appropriate wavelengths for measuring differentially the increase of absorption at 760 nm; the decrease of absorption at 850 nm on deoxygenation of hemoglobin rejecting the common mode change when the difference of the two is taken; and 805 nm is used for blood volume monitoring (26).

the LED at 4 cm distance, so that 8 locations over a 9-cm diameter area from a breast can be measured. The 4-cm source-detector distance gives a banana-shaped pattern revealed by Monte Carlo simulation (5) which demonstrates a high probability of photons at a 4-cm depth in which the diffusion pattern is  $\sim 20$  cm long on the average and gives a significant probability of tumor detection at 4 or more cm depth, as has been verified by CT scans in the case of human brain hematomas (30) and in transabdominal detection of fetal brain saturation in utero (31) in which the fetus was  $> 5$  cm deep in a variety of subjects with varying layers of overlying tissue and most recently in a transthoracic determination of myocardial saturation (31,32). The nomogram display of Figure 2 below illustrates the wide variety of tumor diameters in a

study in which no data were rejected on account of low signal-to-noise ratio. Thus, we conclude that the tumor detectability over the study of 44 cancers and 116 subjects was not flawed by lack of cancer detectability with tumor-to-tissue signal ratio of  $\sim 2$  X for the angiogenesis signal.

The light sources are flashed alternately 20 times per second and electronic circuits are designed to amplify and time-separate the signals in a "sample and hold" circuit which integrates the signals over an interval of a few seconds sufficiently rapidly to follow the movements of the sensor over the breast, allowing usually 10 seconds for any particular sensor position. The data are then digitized and presented as a running time display so that the operator can be sure that stable readings are reached at each

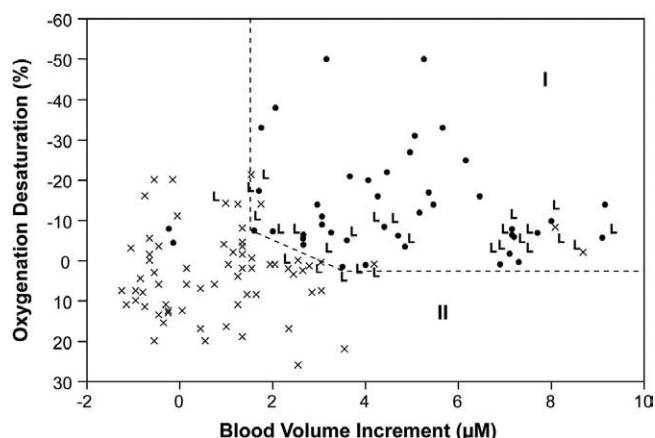


**Figure 2.** A two-dimensional nomogram display of currently available NIR breast cancer data. The abscissa is relative increments of blood concentration in units of micromolar concentration change with respect to the average cancer-free value. The ordinate represents incremental change with respect to the average cancer-free value in percent change of hemoglobin saturation. The reference values (zero for saturations and blood volumes) are based on the contralateral cancer-free breast as represented by a congruence. The wavelengths are at 760 and 850 nm, and the incremental concentrations are appropriately processed for the weighted sum and difference quantities for blood concentration and saturation change, respectively, with 70% and 50  $\mu\text{M}$  the reference points (0) for the two metrics. The data cover studies from 1997 to 2003. Verified cancers are indicated with a dot and cancer-free breasts plotted with an X. Data from Leipzig are marked L, data from Philadelphia are not marked. The nomogram is divided into two parts, one containing the verified cancers (I) and the other containing the cancer-free breasts (II).

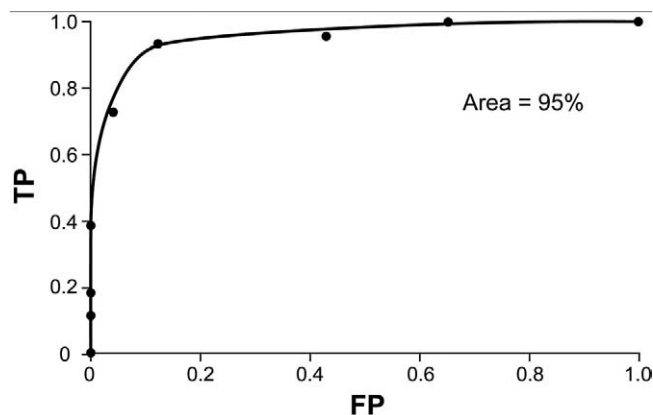


**Figure 3.** ROC/AUC of the Cancer Zone (Zone I) in Figure 2.

position of the sensor (19,32). The particular version of the apparatus shown in Fig. 1 includes pressure transducers so that the effect of pressure on hemodynamics can be precisely monitored and it is expected that this will decrease the variability of the results obtained with manual estimations of pressure (28).

**Methods of Procedure**

*Data Acquisition.*—Skill was required to ensure that all sensors were pressed upon the breast with equal pressure (~3 mmHg) (28,33). Patients were made to lie on their backs and the puck was placed on the breast in such a way that coronal breast scan data was acquired (perpendicular to gravity).

*The Cancer-Free Reference Signals.*—The light intensity from the 8 detectors was adjusted to be near 1 volt by gains set and calibrated with a phantom with known absorption and scattering coefficients ( $\mu_a = 0.04$  to  $0.07$  and  $\mu_s' = 8 \text{ cm}^{-1}$ ). The puck was then transferred to the contralateral breast to include the mirror image location of the suspected cancer. The signal outputs from all source-detector combinations were recorded. The probe was then moved from the contralateral breast to the ipsilateral breast suspected of cancer. The sensors giving the largest changes with respect to the mirror image position on the contralateral breast were related to the suspected cancer. The procedure required less than 10 minutes.

**Data Analysis**

In order to validate the utility of the method described above, we have used an appropriate blood model for three purposes:

1. to establish the blood concentration metric,
2. to establish that the saturation metric was approximate, and
3. to establish that there was minimal cross-talk between the two.

It was found that the following equations were needed for point 3 as determined not only by the concentration and saturation of hemoglobin but by increments of blood volume added to a system set at 50% to 70% saturation (33) (the expected nominal value for tumor oxygen saturation with the blood concentration set in the region of 50  $\mu\text{M}$ ).

This calibration resulted in the following two equations for blood concentration and oxygen saturation with minimal cross-talk between the two. The concentrations may be computed using  $\Delta\epsilon \approx 1 \text{ cm}^{-1}$  and  $\Delta L = 4 \text{ cm} \times 5$  for pathlength factors of 5,  $\Delta OD = \Delta\epsilon \cdot \Delta C \cdot \Delta L$  where OD = optical density,  $\epsilon$  = extinction coefficient, C = concentration, and L = the mean pathlength of photons.

$$\Delta BV \propto 0.3 \cdot \Delta OD730 + \Delta OD850 \tag{1}$$

$$\Delta Deoxy \propto 1.3 \cdot \Delta OD730 - \Delta OD850 \tag{2}$$

In order to demonstrate the utility of the two proposed parameters, relative angiogenesis and relative hypermetabolism, we have followed processes of data analysis and calibration procedures to quantitate blood volume concentration (BV) and % relative oxygenation (%Deoxy). The concentrations of Hb (deoxy hemoglobin) and HbO<sub>2</sub> (Oxy hemoglobin) were calculated by a modified Beer-Lambert

Law,  $\Delta OD = \log \frac{I_o}{I_n}$  where I is light intensity after absorption and scattering and I<sub>0</sub> is the baseline taken from the contralateral breast, using known extinction coefficients of Hb, HbO<sub>2</sub> and differential pathlength factors (DPF) of 7-8 (34).  $\Delta BV$  and  $\Delta \%Deoxy$  were calculated by the proportionalities

$$\Delta BV \propto \Delta[Hb] + \Delta[HbO_2] \quad (3)$$

$$\Delta Deoxy \propto \Delta[HbO_2] - \Delta[Hb] \quad (4)$$

Note that  $\Delta BV$  and  $\Delta Deoxy$  were based on a lipid blood oxygen model. Thus the increments of BV and Deoxy are relative to the contralateral breast:

$$\Delta BV_{\text{tumor}} - \Delta BV_{\text{contra}} \quad (5)$$

$$\Delta Deoxy = \Delta Deoxy_{\text{tumor}} - \Delta Deoxy_{\text{contra}} \quad (6)$$

where  $\Delta BV_{\text{tumor}}$ ,  $\Delta BV_{\text{contra}}$  are  $\Delta BV$  in the tumor breast and the mirror image position of the contralateral breast, respectively, and  $\Delta Deoxy_{\text{tumor}}$ ,  $\Delta Deoxy_{\text{contra}}$  are  $\Delta Deoxy$  in the tumor breast and the mirror image position of the contralateral breast, respectively. We further converted oxygenation to % relative oxygenation (see above values of  $\epsilon$ , C, L).

The average value of hemoglobin saturation for non-cancer tissue is taken to be ~70% (32,33). However, the nomogram display allows the merging of datasets based upon the mean value of the cancer-free breast. This value of 70% is marked zero on the ordinate of Figure 2 and is an approximate average value for the cancer-free breasts shown in Figure 2. Both "zero references" for cancer-free subjects can exhibit demographic variation. An average value as determined optically (mainly arteriolar, capillary, venular vessels) is approximately 25  $\mu M$  and this value is taken to be the Zero point on the abscissa. However, in both axes, the cancer-free breast tissue optical values are set to zero (usually the contralateral mirror image tissue value) and deviations are due to angiogenesis and hyper-

metabolism of the cancer. In this way the effect of demographic and other changes upon the cancer detection are minimized and an otherwise obscured diagnostic capability emerges based on the incremental cancer values with respect to cancer-free values (35).

Sensitivity, specificity and AUC/ROC (area under the ROC curve) were calculated using 2D angiogenesis/hypermetabolism nomograms by using incremental BV and %Sat (36).

## RESULTS

All verified cancers covering studies from 1997 to 2003 are plotted in the 2D nomogram display of BV – %Sat relationship (Figure 2A).

We have been able to summarize our data in the ROC diagram (Fig. 3). The calculated sensitivity, specificity, PPV and NPV are appended in Table 1 (36).

To accommodate data from others' studies, this nomogram is in relative terms with 0 for incremental blood volume and decremental saturation based upon the mean value of the normal population. With this formulation, angiogenesis and hypermetabolism would identify the cancers and segregate them in the upper right portion of the chart and the noncancers on the lower left portion. It is seen that this survey appears to be in accordance with that segregation and therefore the upper right portion has been identified by a box enclosing nearly all of the cancerous breasts, leaving the bulk of the noncancerous breasts in the lower left portion of the diagram.

### False Positives and Negatives

All 6 "out of box" readings are within the zonation of the nomogram. The cancer box contains 4 noncancer patients and the noncancer box contains 2 cancer patients. The 4 false positives in the cancer box are very near the margins of the noncancer box and 2 are low blood volume but high desaturation. A small error in determination of the blood volume increment of roughly 0.2 micromolar is involved. The two false negatives are identified as small cancers, 6 and 7 mm, in which the blood volume increment is significantly underestimated while the deoxygenation is significant.

### Population Differences

The Leipzig population (marked with L) shows a wide blood volume distribution and a small increment of desaturation. In another article we showed correlations of

**Table 1**  
**Summary of Statistics of Relative Oxygenation/Blood Volume Concentration for Figure 2**

ROC/AUC	95%
Sensitivity	96%
Specificity	93%
PPV	89%
NPV	97%

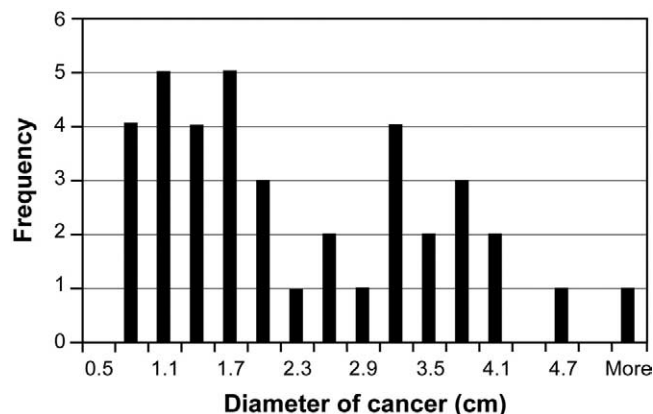


**Figure 4.** Histogram of tumor size for those verified breast cancers for which size data are available, 38 breast cancers detected by NIR hand held "puck."

the optical determination of desaturation with the Eppendorff needle electrode determinations of tissue oxygen concentration in collaboration with Dr. P. Vaupel (38,39, and unpublished data). The zero point of blood concentration is 50  $\mu$ M blood and the zero point of saturation is 70%.

### Operator Differences

Both in Philadelphia and in Leipzig, the data were acquired by more than one operator; the instruments were electronically identical.

### Breast Size

In order to give an indication of the range of breast cancer sizes, Fig. 4 provides a histogram display of the diameters of the tumors examined as obtained from mammography and histopathologically verified cancers.

Figure 4 displays the distribution of sizes of the detected cancers for which size data are available. Most were under 2 cm in diameter. It is limited at the low end by the fact that the mammography does not readily detect cancers below 8 mm in diameter and in the future, MRI

will be used in order to define the lower limiting size for the detection of angiogenesis and hypermetabolism by the NIR system with source-detector separations that may exceed the 4 cm used here.

The high blood volume content of cancers is in agreement with Folkman's ideas of angiogenic activities of tumors (3) and the hypoxic regions of tumors are in accordance with Vaupel's oxygen electrode data (38). Intes recently published similar studies but reported data on an absolute basis (35). It should be emphasized that special care has been taken here to employ blood lipid models with variable blood volume and saturation to ensure minimizations of crosstalk between increase of blood volume and decrease of saturation.

## DISCUSSION

This multicenter study has demonstrated a simple, economical, and patient-friendly NIR breast cancer detector with a multi-wavelength, multi-detector system that gives incremental values of angiogenesis and hypermetabolism, and that is proven to give an ROC/AUC of 95%. The 2-parameter nomogram display of Figure 4 illustrates the total databank obtained over the several years of studies at the University of Pennsylvania in Philadelphia and at Leipzig. The nomogram display contains two zones, Zone I in which relative angiogenesis/hypermetabolism predominates, and Zone II, cancer-free breasts in which neither metric predominates. The usefulness of this 2D nomogram in comparing data over a range of demographics is also demonstrated by other laboratories (35,39).

A novel concept of angiogenesis and hypermetabolism which is complementary to the focus on morphological characteristics of cancer employed by the anatomical approach of ultrasound, X-ray mammography, and MRI is to focus on two biochemically, physiologically based characteristics of cancer not heretofore employed as a diagnostic, namely the spatial correlation of incremental values of total hemoglobin and deoxygenation of hemoglobin, predominantly in the arteriolar, venular, and capillary bed of breast cancers that are incremental with respect to the mirror image location on the contralateral breast. The NIR optical information is in the form of magnitudes rather than shapes, a considerable distinction between the NIR optical method (31,32,34) and the morphologically based X-ray mammography (41), ultrasound (42), and MRI (40).

With regard to hypermetabolism NIRS can detect with low oxygen concentration, and PET detection with FDG (43) uses the same concept of lack of oxygen metabolism. Taking into account the work of Vaupel (38) and others indicating that, in spite of intense angiogenesis, a growing cancer may still be underserved with oxygen because of the faulty nature of the vessels and the oxygen demand of growth, to the extent that glycolytic activity may be stimulated as originally observed by Otto Warburg (1) and studied further by us as Krebs' Crabtree's effect. It seems therefore reasonable that the increment of the blood flow might be correlated with the decrease of oxygen saturation and that a coordinated plot of the two might be useful. On this basis, relative rather than absolute values may be adequate in NIRS and previous study suggests excessive between-subject effects (37). Large variables of the bulk optical property of the breast suggest the use of internal reference rather than absolute values of the optical properties (45).

Although by using selected wavelengths sufficient sensitivity and specificity are obtained in these studies to provide a highly significant ROC/AUC score, this CWS method is less sensitive to the many demographic factors which influence the properties of the human breast (46) yet which are known in general to influence both breasts equally. One of the key problems of the breast is the wide variety of demographic size, texture, chemical composition, and age (Tromberg, personal communication). Thus, a secure tissue baseline is not available unless it is taken from the adjacent tissue, which is found to be a satisfactory reference and is a feasible standard for cancer detection. One may choose either a portion of the same breast or the mirror image portion of the contralateral breast. The latter may seem to be better since the majority of breasts are highly symmetrical. For this reason we propose as our standard baseline metric, mirror image portion of the contralateral breast. If a priori information is available, for example, by palpation, ultrasound, or mammography, the NIR device may be placed directly on the surface projection of the cancer. The work of others, particularly Tromberg (47), Cubbedu (47), Vaupel (49), and Yamashita (49) have suggested that the use of other metrics such as water, lipid, and light scattering could afford increases in AUC multi-dimensional plots of the type used here. However, none of these is known to be directly related to the biochemical, physiological properties of tumor growth as are the two parameters se-

lected here. However, other biochemical characteristics may be employed, for example the concentration of intracellular compounds related to lipid biosynthesis or, indeed, the impact of growth and its concomitant energy demand upon the cancer bioenergetics (48).

The addition of further metrics, combined with higher spatial resolution, should increase further the ROC/AUC values and at the same time give better quantitation of the optical characteristics of deep small tumors. However, the high throughput, simplicity of operation, and the convenience of this device make it worthwhile to proceed with further studies to improve the breast sensor contact problem by contact pressure sensing or eliminate the problem by flying spot non-contact, remote sensing of the optical signals (17). In the later case, higher resolution imaging can be readily obtained by flying spot and phased array systems (17,23,24) from all geometric aspects of the breast. Such a manifold of source and detector positions proposed must decrease the throughput and increase the complexity of the device. Further, the frequency of occurrence of small cancers and precancers is low, e.g., in the Hospital of the University of Pennsylvania (HUP) BRCA1/2 study, fewer than 1% of those in the high-risk category initially exhibit a detectable cancer (44).

Each breast cancer detection method (MRI, ultrasound, optical tomography) may have its own niche in health care delivery, the larger more complex devices as a part of Radiological Services and the small devices for clinics specializing in early detection of cancer, and even for personal healthcare as befits underserved, noncompliant populations (50). There are a number of intrinsic signals that are under investigation elsewhere that may be quite useful. Water content is readily accessible optically, as are scattering, lipid, and pigment. If exogenous probes are to be considered, ICG affords not only increased tumor-to-tissue ratio, but also a measure of diagnostic capability. Finally, molecular beacons responsive to the energy demands of tumor growth, particularly fluorescent glucose, by analogy to radioactive glucose, may add to the sensitivity and specificity of cancer detection on a biochemical/physiological basis. Thus, a very large number of factors will increase the sensitivity and specificity of cancer detection by optical means. While incremental changes of angiogenesis and hypermetabolism are small, much larger tumor-to-tissue ratios can be expected of extrinsic signals, ICG, fluorescent glucose, and genetically directed molecular beacons.

## Relation to Other Studies

While a general consensus has been reached that angiogenesis gives a high blood volume signal, results seem to be inconsistent with respect to the blood saturation level of cancer. We believe due to the lack of blood models that vary both blood volume and blood O<sub>2</sub> saturation, that separation of the blood volume signal from the saturation signal is important, and that an increase of blood volume, causing an increase of oxy hemoglobin, will adversely affect the calculation of desaturation of hemoglobin. In fact, the usual equations for calculating saturation do not take into account the possibility of crosstalk from other signals as does our empirical equation (13,35,39).

## Effect of Cancer Type

Since our approach is based upon two biochemical/physiological properties of breast cancers, the structural, architectural, and histopathological features which may be used to classify cancers have been found less well-correlated with the Figure 3 nomogram. As might be expected, these features are de-emphasized in this survey of biochemical and physiological differences of growing cancers relative to the corresponding cancer-free tissue. Thus, commonality of factors involved in the biochemistry of tumor growth is expected from these studies while structural features of different kinds of tumors would be de-emphasized by the use of relative values for the baseline, emphasizing the difference between this approach and one based upon morphological characteristics involving spiculation, lobulation, and other demographic features of the cancers (41,42,46).

## Future Developments

A measure of success based upon a nomogram of two intrinsic features of breast cancer can be improved by other metrics that correspond physiologically or biochemically to growth stimuli (26,51).

## REFERENCES

1. Warburg O. *Biochem Z* 1926; 177:471-486.
2. Zhao Z, Zhang J, Nioka S, Dong L, Du J, Wen S, Chance B. Blood flow and oxygen saturation changes according to pressure effect in NIR breast cancer imaging study. *SPIE Proceedings Vol. 5693 Optical tomography and spectroscopy of tissue VI* (Chance B, Alfano RR, Tromberg BJ, Tamura M, Sevick-Muraca EM, eds.) Bellingham, WA: SPIE, 2005; 271-277.
3. Chance B, Castor LN. Some patterns of the respiratory pigments of Ascites tumors of mice. *Science* 1952; 116:200-202.
4. Folkman J. Tumor angiogenesis: therapeutic implications. *N Engl J Med* 1971; 285:1182-1186.
5. Lin Y, Lech G, Nioka S, Intes X, Chance B. Noninvasive, low-noise, fast imaging of blood volume and deoxygenation changes in muscles using light-emitting diode continuous-wave imager. *Rev Sci Instrum* 2002; 73:3065.
6. Patterson MS, Chance B, Wilson BC. Time resolved reflectance and transmittance for the noninvasive measurement of tissue optical properties. *J Appl Optics* 1989; 28:2331-2336.
7. Cutler M. Transillumination of the breast. *Surg Gynecol Obstet* 1929; 48:721-727.
8. Girolamo RF, Gaythorpe JV. Clinical diaphanography—Its present perspective. *Crit Rev Oncol Hematol* 1984; 2:1-31.
9. Millikan GA. Experiments on muscle haemoglobin *in vivo*; The instantaneous measurement of muscle metabolism. *Proc Roy Soc London B* 1937; 129:218-241.
10. Millikan GA. The oximeter, an instrument for measuring continuously the oxygen saturation of arterial blood in man. *Rev Sci Instrum* 1942; 13:434.
11. Chance B. Stable spectroscopy of small density changes. *Rev Sci Instrum* 1947; 18:601-609.
12. Chance B, Williams GR. Respiratory enzymes in oxidative phosphorylation. II. Difference spectra. *J Biol Chem* 1955; 217:395-408.
13. Yodh A, Chance B. Spectroscopy and imaging with diffusing photons. *Phys Today* 1995; 48:34-40.
14. Cheng Z, Mao JM, Bush R, Kopans DB, Moore RH, Chorlton M. Breast cancer detection by mapping hemoglobin concentration and oxygen saturation. *Appl Opt* 2003; 42:6412-6421.
15. Jakubowski DB, Cerussi AE, Bevilacqua F, Shah N, Hsiang D, Butler J, Tromberg BJ. Monitoring neoadjuvant chemotherapy in breast cancer using quantitative diffuse optical spectroscopy: a case study. *J Biomed Opt.* 2004 Jan-Feb;9(1):230-8.
16. Hamaoka T, Albani C, Chance B, Iwane H. A new method for the evaluation of muscle aerobic capacity in relation to physical activity measured by near-infrared spectroscopy. In Saito Y, Portmans J, Hashimoto I, Oshida Y, eds: *Integration of Medical and Sports Sciences Basel*: Karger, 1992, vol. 37, p. 421-429.
17. Gratton E, Mantulin WW, vandeVen MJ, Fishkin JB, Maris M, Chance B. The possibility of a near-infrared optical imaging system using frequency domain methods. *Proceedings of the Third International Conference: Peace through Mind/Brain Science* (Aug. 5-10), Hamamatsu, Japan, 1990; pp. 183-189.
18. Kang KA, Chance B, Zhao S, Srinivasan S, Patterson E, Troupin R. Breast tumor characterization using near-infrared spectroscopy. *SPIE Proceedings Vol. 1888 Photon Migration and Imaging in Random Media and Tissues* (Chance B., Alfano RR, eds.) Bellingham, WA: SPIE, 1993; 487-499.
19. Chance B, Tamura T. Spatial and temporal resolution of frontal cognitive response using NIR tomography. *International Symposium of Brain Mapping OISO '96* (Sept. 13-15), Oiso, Japan, 1996; p. S-III-4.
20. Chance B, Dait MT, Chang C, Hamaoka T, Hagerman F. Non-invasive evaluation of deoxygenation during intense exercise and recovery of oxygenation of hemoglobin and myoglobin in the quadriceps muscles of elite competitive rowers. *Am J Physiol* 1992; 262:C766-C775. BC brain.
21. Chance B. NIR responses of the human forebrain (Brodmann's 9 and 10) to physiological function. *SPIE Proceedings Vol. 5693 Optical tomography and spectroscopy of tissue VI* (Chance B, Alfano RR, Tromberg BJ, Tamura M, Sevick-Muraca EM, eds.) Bellingham, WA: SPIE, 2005; 166-171.
22. Chance B, Onaral B, Pourrezai, Herr M. A new approach to early detection for women's medicine. *Era of Hope Department of Defense Breast Cancer Research Program Meeting Proceedings*. Philadelphia, PA: Department of the Army, 2005; 48.
23. Zhang J, Lin Y, Nioka S, O'Connor N, Czerniecki B, Conant EF, Chance B. Application of LED device for breast cancer diagnosis, *Proc SPIE* 2002; 4916:30-36.
24. Chance B, Kang K, He L, Weng J, Sevick E. Highly Sensitive object location in tissue models with linear in-phase and anti-phase multi-element optical arrays in one and two dimensions. 1993. *Proc Natl Acad Sci USA* 1993; 90:3423-3427.
25. Chen Y, Zheng G, Zhang ZH, Blessington D, Zhang M, Li H, Liu Q, Zhou L, Intes X. Metabolism-enhanced tumor localization by fluorescence imaging: *in vivo* animal studies. *Optics Lett* 2003; 28:2070-2072.

26. Vo-Dinh T. *Biomedical Photonics Handbook*. Boca Raton, FL: CRC Press, 2003.
27. Chance B. The optical method. *Annu. Rev Biophys Biophys Chem* 1991; 20:1-18.
28. Zhou S, Huang S, Xie C, Long H, Nioka S, Chance B. Optical imaging of breast tumor by using dual wavelength amplitude cancellation system (phased array). In: Sevick-Muraca EM, Izatt JA, Ediger MN, eds. *OSA Trends in Optics and Photonics, Vol. 22. Biomedical Optical Spectroscopy and Diagnostics/Therapeutic Laser Applications*. Washington, DC: Optical Society of America, 1998; 197-200.
29. Nioka S, Wen S, Zhang J, Du J, Intes X, Zhao Z, Chance B. Simulation study of breast tissue hemodynamics during pressure perturbation. *Adv Exp Med Biol*. 2005 in press.
30. Fukui Y, Ajichi Y, Okada E. Monte Carlo prediction of near-infrared light propagation in realistic adult and neonatal head models, *Appl Opt* 2003; 42:2881-2887.
31. Gopinath SP, Robertson CS, Contant CF, Narayan RK, Grossman RG, Chance B. Early detection of delayed traumatic intracranial hematomas using near-infrared spectroscopy. *J Neurosurg* 1995; 83:438-44.
32. Choe R, Durduran T, Yu G, Nijland MJ, Chance B, Yodh AG, Ramanujam N. Transabdominal near infrared oximetry of hypoxic stress in fetal sheep brain in utero. *Proc Natl Acad Sci U S A*. 2003; 100:12950-12954.
33. Chance B, Nioka S, Cappola T, Margulies K. NIR imaging of fetal brain and adult myocardium. The 46<sup>th</sup> Experimental Nuclear Magnetic Resonance Conference, April 10-15, 2005, Rhode Island Convention Center, Providence, RI.
34. Smith DS, Levy W, Maris M, Chance B. Reperfusion hyperoxia in brain after circulatory arrest in humans. *Anesthesiology* 1990; 73:12-19.
35. Fantini S, Hueber D, Franceschini MA, Gratton E, Rosenfeld W, Stubblefield PG, Maulik D, Stankovic MR. Non-invasive optical monitoring of the newborn piglet brain using continuous-wave and frequency-domain spectroscopy. *Phys Med Biol* 1999; 44:1543-1563.
36. Intes X, Djeziri S, Ichalalene Z, et al. Time-domain optical mammography SoftScan<sup>®</sup>: initial results. *Acad Radiol* 2005; In Press.
37. Campbell MJ, Machin D. *Medical Statistics* 3rd ed. Wiley, 1999, pp. 43-46.
38. Thews O, Li Y, Kelleher DK, Chance B, Vaupel P. Microcirculatory function, tissue oxygenation, microregional redox status and ATP distribution in tumors upon localized infrared-A-hyperthermia at 42 degrees C. *Adv Exp Med Biol* 2003; 530:237-47.
39. Vaupel P, Schlenger K, Knoop C, Hockel M. Oxygenation of human tumors: evaluation of tissue oxygen distribution in breast cancers by computerized O<sub>2</sub> tension measurements. *Cancer Res* 1991; 51: 3316-3322.
40. Grosenick D, Wabnitz H, Moesta KT, et al. Concentration and oxygen saturation of haemoglobin of 50 breast tumours determined by time-domain optical mammography. *Phys Med Biol* 2004;7:49, 1165-81.
41. Ntziachristos V, Yodh A, Schnall M, Chance B. MRI-Guided diffuse optical spectroscopy of malignant and benign breast lesions. *Neoplasia* 2002; 4:347-354.
42. Li A, Miller E, Kilmer M, et al. Tomographic optical breast imaging guided by three-dimensional mammography. *Appl Opt* 2003; 42:5181-5190.
43. Zhu Q, Huang MM, Chen NG, et al. Ultrasound-guided optical tomographic imaging of malignant and benign breast lesions: initial clinical results of 19 cases. *Neoplasia* 2003; 5:379-388.
44. Alavi A, Kung JW, Zhuang H. Implications of PET based molecular imaging on the current and future practice of medicine. *Semin Nucl Med* 2004; 34:56-69.
45. Pogue BW, Jiang S, Dehghani H, et al. Characterization of hemoglobin, water, and NIR scattering in breast tissue: analysis of intersubject variability and menstrual cycle changes. *J Biomed Opt* 2004; 9:541-552.
46. Durduran T, Choe R, Culver JP, et al. Bulk optical properties of healthy female breast tissue. *Phys Med Biol* (2002); submitted
47. Tromberg BJ, Shah N, Lanning R, et al. Non-invasive in vivo characterization of breast tumors using photon migration spectroscopy. *Neoplasia* 2000; 2(1-2): 26-40.
48. Torricelli A, Spinelli L, Pifferi A, Taroni P, Cubbedu R. Use of a nonlinear perturbation approach for in vivo breast lesion characterization by multiwavelength time-resolved optical mammography. *Opt Express* 2003;11 p. 853.
49. Vaupel P, Hockel M. Blood supply, oxygenation status and metabolic microclimate of breast cancers: characterization and therapeutic relevance. *Int J Oncol* 2000; 17:869-879.
50. Suzuki K, Yamashita Y, Ohta K, Chance B. Quantitative measurement of optical parameters in the breast using time-resolved spectroscopy: Phantom and preliminary in vivo results. *Invest Radiol* 1994; 29:410-4.
51. Armstrong K, Weber BL. Breast cancer screening for high-risk women: too little, too late? *J Clin Oncol* 2001. Feb 15;19:919-20.